

Cite this: *RSC Adv.*, 2017, 7, 11510

# $\text{H}_3\text{PW}_{12}\text{O}_{40}$ supported on functionalized polyoxometalate organic–inorganic hybrid nanoparticles as efficient catalysts for three-component Mannich-type reactions in water†

Roushan Khoshnavazi,\* Leila Bahrami, Forugh Havasi and Elham Naseri

Two new types of catalyst were synthesized by the immobilization of  $\text{H}_3\text{PW}_{12}\text{O}_{40}$  (HPW<sub>12</sub>) on the surface of organic–inorganic polyoxometalate nanoparticles of  $\text{H}_6\text{Cu}_2[\text{PPDA}]_6[\text{SiW}_9\text{Cu}_3\text{O}_{37}] \cdot 12\text{H}_2\text{O}$  (HybPOM) (PPDA = *p*-phenylenediamine) and  $\text{Go}/\text{Fe}_3\text{O}_4/\text{HybPOM}$  nanoparticles. These catalysts were characterized by thermogravimetric analysis (TGA), Fourier transform infrared (FT-IR) spectroscopy, scanning electron microscopy (SEM), energy dispersive X-ray analysis (EDX) and alternating gradient force magnetometry (AGFM). The IR spectroscopy as well as XRPD reveal that HPW<sub>12</sub> were immobilized on the support. The potentiometric titration with *n*-butylamine reveal that the catalysts can be classified as strong acids. The results show that the particles are mostly spherical in shape and have an average size in the range of 20–50 nm. The catalytic activities of the catalysts were probed through one-pot three-component Mannich-type reactions of aldehydes, amines and ketones in water at room temperature. The catalysts were re-used at least five times without any loss of their high catalytic activity.

Received 29th November 2016

Accepted 8th February 2017

DOI: 10.1039/c6ra27519b

rsc.li/rsc-advances

## 1. Introduction

Polyoxometalates (POMs), discrete anionic metal-oxo clusters, can be linked together through cationic moieties to build materials with incredible structural diversity which exhibit a wide variety of compositions and structural versatility,<sup>1–3</sup> as well as important optical,<sup>4</sup> catalytic,<sup>5–9</sup> and magnetic<sup>10–13</sup> properties. POM clusters occupy a vast parameter space between the mononuclear metalate species and the bulk oxide.<sup>14</sup> POMs can also self-assemble into ordered patterns at the nanometer scale, and thus have multilevel ordered structures.<sup>15,16</sup> The great diversity in structure and composition of POMs make them attractive materials in many fields.<sup>17</sup> One focus is to use them as both homogeneous and heterogeneous catalysts in oxidation and acid promoted reactions. Heteropoly acids (HPAs) such as  $\text{H}_3\text{PW}_{12}\text{O}_{40}$  have been extensively studied as acid catalysts for many reactions. Despite the above advantages, use of POMs is restricted owing to the fact that they are non-porous solids with low surface area (of less than  $10 \text{ m}^2 \text{ g}^{-1}$ ). Because of their ionic nature they dissolve well in polar solvents such as water, alcohols, ketones, acetonitrile and dimethylsulfoxide which makes them difficult to separate from the reaction products and their inevitable loss during recycling. Hence, efforts have also been

made to study the support of HPAs on inert or weak acidic high surface area materials such as, silica,<sup>18</sup> zeolite,<sup>19</sup> and alumina.<sup>20</sup> The application of supported HPAs increases the specific surface area of the catalysts and modifies their catalytic properties. Thus, immobilization of HPAs on supports show a greater number of surface acid sites than their bulk components. The use of nanoparticles (NPs) offers many advantages for supporting homogeneous catalysts due to their unique size and physical properties. NPs could have a higher catalyst loading capacity and a higher dispersion than many conventional support matrices. Recently, supported HPAs have been developed for a wide range of organic reactions in fundamental research.<sup>21,22</sup>

Easier recovery and recycling after carrying out reaction through simple separation processes are the advantages that supported HPAs have compared to homogeneous examples. In addition, heteropoly acids are more active catalysts for various reactions in solution than conventional inorganic and organic acids and they have many environmental benefits. They were tested as catalysts for several reactions with the final objective of industrial use,<sup>23–25</sup> as alcohol dehydration,<sup>26</sup> alkylation<sup>27</sup> or esterification<sup>28</sup> reactions. Among heteropoly acids, 12-tungstophosphoric acids are the most widely used catalysts owing to their high acid strength and thermal stability, and relatively low reducibility. Recently, the supported heteropoly acids as heterogeneous catalysts have attracted much attention.  $\text{H}_3\text{PW}_{12}\text{O}_{40}$  have been immobilized on  $\text{Fe}_3\text{O}_4$  functionalized nanoparticles<sup>29–31</sup> and successfully

Department of Chemistry, University of Kurdistan, P.O. Box 66135-416, Sanandaj, Iran. E-mail: r.khoshnavazi@uok.ac.ir; khoshnavazi@yahoo.com; Fax: +98 87 33624133; Tel: +98 87 33624133

† Electronic supplementary information (ESI) available. See DOI: 10.1039/c6ra27519b

applied as active species in organic reaction catalysis.<sup>32,33</sup> In this study, organic–inorganic nanohybrid of HybPOM was used as a new kind of high surface area material for supporting homogeneous  $\text{H}_3\text{PW}_{12}\text{O}_{40}$ . The functionalized organic–inorganic polyoxometalates of HybPOM was synthesized by a simple and high yield reaction.<sup>34</sup> Ultimately, mixing a suspension of HybPOM with an ethanolic solution of  $\text{HPW}_{12}$  leads to the formation of HybPOM/ $\text{HPW}_{12}$  NPs which involves the reaction of  $\text{H}_3\text{PW}_{12}\text{O}_{40}$  with surface amine groups of HybPOM. Protonation of amine groups gives positively charged cations which bound electrostatically to the heteropolyanions.

Despite the high surface areas of HybPOM/ $\text{HPW}_{12}$ , filtration or centrifugation is needed and the separation process is still a difficult and time consuming process. Magnetic nanoparticles are excellent supports for various catalysts<sup>35,36</sup> and can easily be separated and recycled from the products by an external magnet. Surface functionalized  $\text{GO}/\text{Fe}_3\text{O}_4$  nanoparticles are a kind of novel functional material which has been widely used in biotechnology and catalysis. The  $\text{GO}/\text{Fe}_3\text{O}_4/\text{HybPOM}$  magnetic nanoparticle was synthesized simply by addition of HybPOM to the ethanol disperse solution of  $\text{GO}/\text{Fe}_3\text{O}_4$  nanoparticle. The GO because of its exceptionally high surface area ( $2630 \text{ m}^2 \text{ g}^{-1}$ ) and abundant oxygenate groups such as epoxy, hydroxyl, and carboxyl groups on their surface, is as an ideal support for immobilizing and improving POMs catalytic activity. The  $\text{GO}/\text{Fe}_3\text{O}_4$  nanoparticle, has key properties such as magnetic separation, the large surface area and ease of functionalizing with various chemical groups to increase their dependence toward target compounds. Through a nucleophilic attack by available  $\text{NH}_2$  groups on the surface HybPOM hybrid with functional groups such as epoxy, hydroxyl, and carboxyl groups on the surface of  $\text{GO}-\text{Fe}_3\text{O}_4$  magnetic nanoparticle, the hybrid material is grafted *via* C–N bond formation.<sup>34</sup> Once again mixing a suspension of the  $\text{GO}/\text{Fe}_3\text{O}_4/\text{HybPOM}$  with an ethanolic solution of  $\text{HPW}_{12}$  lead to the formation of  $\text{GO}/\text{Fe}_3\text{O}_4/\text{HybPOM}/\text{HPW}_{12}$  NPs.

The prepared  $\text{GO}/\text{Fe}_3\text{O}_4/\text{HybPOM}/\text{HPW}_{12}$  hybrid composite can be easily separated by magnetic separation from the medium after reaction. The  $\text{GO}/\text{Fe}_3\text{O}_4/\text{HybPOM}/\text{HPW}_{12}$  hybrid composite show the same catalytic efficiency compared to the HybPOM/ $\text{HPW}_{12}$  and can be easily manipulated by external magnetic field.

In this paper, we synthesized HybPOM/ $\text{HPW}_{12}$  and  $\text{GO}/\text{Fe}_3\text{O}_4/\text{HybPOM}/\text{HPW}_{12}$  nanoparticles by immobilization of Keggin type heteropoly acid  $\text{H}_3\text{PW}_{12}\text{O}_{40} \cdot x\text{H}_2\text{O}$  on organic–inorganic nano hybrid of  $\text{H}_6\text{Cu}_2[\text{PDA}]_6[\text{SiW}_9\text{Cu}_3\text{O}_{37}] \cdot 12\text{H}_2\text{O}$  (HybPOM) and nanocomposite of  $\text{GO}/\text{Fe}_3\text{O}_4/\text{HybPOM}$  nanoparticles, respectively and assessed their catalytic activity in Mannich-type reactions in water. Indeed, the venerable Mannich reactions and its variants represent one of the more powerful constructs for alkaloid synthesis.<sup>37</sup> To the best of our knowledge, this is the first report containing immobilization of a heteropolyacid on organic–inorganic nano hybrid. Synthesis, characterization and catalytic application of new nano catalysts have been investigated.

## 2. Experimental section

### Materials and apparatus

All reagents and solvents were commercially obtained and used without further purification. The 12-tungstophosphoric acid ( $\text{H}_3\text{PW}_{12}\text{O}_{40} \cdot x\text{H}_2\text{O}$ ) was prepared according to a reported procedure.<sup>38</sup> The  $\text{GO}-\text{Fe}_3\text{O}_4$  was prepared according to the literature.<sup>39</sup>

Powder XRD was obtained by an X'PertPro Panalytical, Holland diffractometer in 40 kV and 30 mA with a  $\text{CuK}\alpha$  radiation ( $\lambda = 1.5418 \text{ \AA}$ ). Infrared spectra were recorded on a Bruker Vector 22 FT-IR using KBr plate. The morphology of nanocomposites was revealed by a scanning electron microscope (FESEM-TESCAN MIRA3). The elements in the nanocomposite samples were probed energy-dispersive X-ray (EDX) spectroscopy accessory to the FESEM-TESCAN MIRA3 scanning electron microscopy. The magnetic properties were investigated by a home-made alternative gradient force magnetometer (AGFM) in the magnetic field range of  $-5000$  to  $5000 \text{ Oe}$  at room temperature. Thermo gravimetric analysis-differential thermal analysis (TGA-DTA) was carried out using a STA PT-1000 LINSEIS.

### Synthesis of nanohybrids

**Preparation of  $\text{H}_6\text{Cu}_2[\text{PDA}]_6[\text{SiW}_9\text{Cu}_3\text{O}_{37}] \cdot 12\text{H}_2\text{O}$  nanohybrid (HybPOM).** HybPOM was prepared by the following stated method.<sup>34</sup> A  $2.00 \text{ g}$  ( $0.725 \text{ mmol}$ ) of  $\text{Na}_9\text{H}[\beta\text{-SiW}_9\text{O}_{34}] \cdot 18\text{H}_2\text{O}$  was dissolved in water ( $100 \text{ mL}$ ) at room temperature.  $\text{Cu}(\text{C}_2\text{H}_3\text{O}_2)_2 \cdot \text{H}_2\text{O}$  ( $3.00 \text{ g}$ ,  $15 \text{ mmol}$ ) was added to the solution while stirring, resulting in a blue solution. Then,  $0.7 \text{ g}$  ( $6.5 \text{ mmol}$ ) of PPDA was slowly added to this blue solution while stirring, producing a blue-brown precipitate. After stirring for  $4 \text{ h}$ , the precipitate color changed from blue-brown to black. Obtained black precipitate was centrifuged and washed several times with water and acetonitrile, then air-dried at room temperature.

**Preparation of  $\text{GO}/\text{Fe}_3\text{O}_4/\text{HybPOM}$  nanohybrid.**  $\text{GO}/\text{Fe}_3\text{O}_4/\text{HybPOM}$  was prepared as per the following method.<sup>34</sup> To disperse  $\text{GO}-\text{Fe}_3\text{O}_4$  in  $30 \text{ mL}$  of absolute ethanol, an appropriate amount of HybPOM was added and the mixture was sonicated for  $10 \text{ min}$  to form a homogeneous dispersion. Then, the mixture was stirred under reflux condition for  $24 \text{ h}$ . The obtained solid was then magnetically collected from the solution and washed three times with water and ethanol, and dried at  $50^\circ\text{C}$ .

**Preparation of HybPOM/ $\text{HPW}_{12}$  nanohybrid.** A  $0.500 \text{ g}$  of HybPOM was dispersed in  $25 \text{ mL}$  of absolute ethanol by sonication for  $20 \text{ minutes}$ . An appropriate amount of dissolved  $\text{H}_3\text{PW}_{12}\text{O}_{40} \cdot x\text{H}_2\text{O}$  in the absolute ethanol was added to the above solution while stirring. The resulting mixture was stirred under reflux condition for  $48 \text{ h}$ . The crude product was separated by centrifuges, washed several times with ethanol and dried at  $50^\circ\text{C}$  under reduced pressure.

**Preparation of  $\text{GO}/\text{Fe}_3\text{O}_4/\text{HybPOM}/\text{HPW}_{12}$  nanohybrid.**  $0.500 \text{ g}$   $\text{GO}/\text{Fe}_3\text{O}_4/\text{HybPOM}$  was suspended in  $25 \text{ mL}$  of absolute ethanol and then an appropriate amount of  $\text{H}_3\text{PW}_{12}\text{O}_{40} \cdot x\text{H}_2\text{O}$  dissolved in absolute ethanol was added to the suspension while stirring. The mixture was stirred under reflux condition for  $24 \text{ hours}$ . The obtained nanohybrid were magnetically



collected, washed three times with ethanol ( $3 \times 5$  mL), and dried at  $50^\circ\text{C}$  under reduced pressure.

### Titration of the catalysts acidity

The acidity of HybPOM/HPW<sub>12</sub> and Go/Fe<sub>3</sub>O<sub>4</sub>/HybPOM/HPW<sub>12</sub> was probed by potentiometric titration.<sup>40</sup> HybPOM/HPW<sub>12</sub> or Go/Fe<sub>3</sub>O<sub>4</sub>/HybPOM/HPW<sub>12</sub> (0.05 g) was suspended in acetonitrile, and stirred for 3 h. Then, the suspension was titrated with 0.05 M *n*-butylamine in acetonitrile at  $0.05\text{ mL min}^{-1}$ . The electrode potential variation was measured with a WTW digital nanolab model using a double-junction electrode.

### General procedure for the synthesis of $\beta$ -amino ketones catalyzed by HybPOM/HPW<sub>12</sub>

Typically, the catalyst (0.005 g) was added to a mixture of aldehyde (1 mmol), amine (1 mmol), cyclohexanone (2 mmol) and H<sub>2</sub>O (1 mL). The reaction mixture was vigorously stirred at room temperature for an appropriate time. The progress of the reaction was monitored by TLC. After completion of the reaction, the catalyst was separated by centrifuge, washed with ethanol and water, vacuum dried and stored for subsequent runs. The reaction mixture was extracted with H<sub>2</sub>O and EtOAc. The organic layer was dried over MgSO<sub>4</sub> and then evaporated under reduced pressure. This solution was concentrated at room temperature to yield the crude products. The crude products were purified either by crystallization from ethanol, giving of  $\beta$ -amino ketones in good yield. The reaction product was characterized by IR and mass spectroscopy.

### General procedure for the synthesis of $\beta$ -amino ketones catalyzed by Go/Fe<sub>3</sub>O<sub>4</sub>/HybPOM/HPW<sub>12</sub>

Typically, the catalyst (0.007 g) was added to a mixture of aldehyde (1 mmol), amine (1 mmol), cyclohexanone (2 mmol)

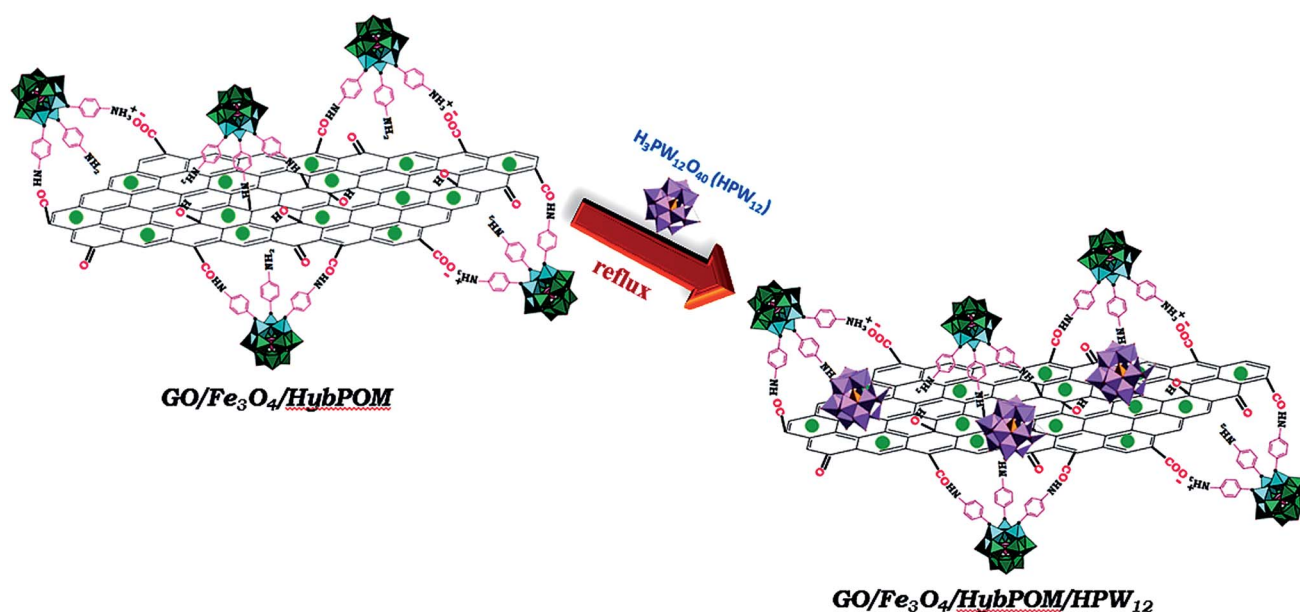
and H<sub>2</sub>O (1 mL). The reaction mixture was vigorously stirred at room temperature for an appropriate time. The progress of the reaction was monitored by TLC. After completion of the reaction, the catalyst was separated by external magnet and washed with ethanol and water, vacuum dried and stored for subsequent runs. The reaction mixture was extracted with H<sub>2</sub>O and EtOAc. The organic layer was dried over MgSO<sub>4</sub> and then evaporated under reduced pressure. The crude products were purified either by crystallization from ethanol, giving of  $\beta$ -amino ketones in good yield.

### Characterization of organic products

**2-(Phenyl(phenylamino)methyl)cyclohexanone** (Table 2, entry 1). White solid, mp  $128\text{--}129^\circ\text{C}$ ;<sup>53</sup> FT-IR (KBr,  $\text{cm}^{-1}$ ) 1440–1594 (C=C, aromatic), 1701 (C=O, carbonyl), 3349 (NH, second amine), 2925, 2860 (C–H, aliphatic), 3015 (C–H, aromatic). <sup>1</sup>H NMR (250 MHz, CDCl<sub>3</sub>)  $\delta$  (ppm): 7.80 (s, 1H), 7.45–7.26 (m, 7H), 6.68–6.64 (m, 2H), 4.80 (d,  $0.38H_{\text{syn}}$ ,  $J = 2.25\text{ Hz}$ ), 4.63–4.60 (m,  $0.36H_{\text{anti}}$ ), 2.94–2.84 (m, 2H), 2.54–2.34 (m, 2H), 1.91–1.77 (m, 4H), 1.25 (s, 1H). (*syn/anti*: 50/50). EI-MS (70 eV):  $m/z$  (%) = 279 ( $M^{+}$ , 11), 182 ( $M^{+} - \text{C}_6\text{H}_9\text{O}$ , 48).

**2-((2-Chlorophenyl)(phenylamino)methyl)cyclohexanone** (Table 2, entry 2). White solid, mp  $137\text{--}139^\circ\text{C}$ ;<sup>54</sup> FT-IR (KBr,  $\text{cm}^{-1}$ ) 1434–1600 (C=C, aromatic), 1704 (C=O, carbonyl), 3380 (NH, second amine), 2933, 2857 (C–H, aliphatic), 3045 (C–H, aromatic); <sup>1</sup>H NMR (250 MHz, CDCl<sub>3</sub>)  $\delta$  (ppm): 7.91 (s, 1H), 7.51–7.40 (m, 3H), 7.33–7.26 (m, 3H), 6.65–6.62 (m, 1H), 6.51 (d, 1H,  $J = 8\text{ Hz}$ ), 5.33 (d,  $0.30H_{\text{syn}}$ ,  $J = 3.25\text{ Hz}$ ), 4.89 (d,  $0.41H_{\text{anti}}$ ,  $J = 4.5\text{ Hz}$ ), 2.77–2.54 (m, 7H), 1.96–1.92 (m, 2H). (*syn/anti*: 42/58); EI-MS (70 eV):  $m/z$  (%) = 315 [ $(M^{+} + 2)$ , 3], 313 ( $M^{+}$ , 9), 216 ( $M^{+} - \text{C}_6\text{H}_9\text{O}$ , 100).

**2-((4-Bromophenyl)(phenylamino)methyl)cyclohexanone** (Table 2, entry 3). White solid, mp  $109\text{--}110^\circ\text{C}$ ;<sup>55</sup> FT-IR (KBr,  $\text{cm}^{-1}$ ) 1484–1610 (C=C, aromatic), 1709 (C=O, carbonyl),



Scheme 1 The schematic pathway for preparing Go/Fe<sub>3</sub>O<sub>4</sub>/HybPOM/HPW<sub>12</sub> hybrid composite.



3380 (NH, second amine), 2927, 2856 (C–H, aliphatic), 3029 (C–H, aromatic);  $^1\text{H}$  NMR (250 MHz,  $\text{CDCl}_3$ )  $\delta$  (ppm): 7.49–7.41 (m, 2H), 7.41–7.39 (m, 2H), 7.26–7.23 (m, 2H), 7.23–7.07 (m, 2H), 6.69–6.64 (m, 1H), 6.51 (d, 1H,  $J = 6$  Hz), 4.72 (d, 0.41H<sub>syn</sub>,  $J = 4$  Hz), 4.58 (d, 0.54H<sub>anti</sub>,  $J = 6.25$  Hz), 2.78–2.76 (m, 1H), 2.53–2.38 (m, 1H), 2.36–2.31 (m, 1H), 1.94–1.71 (m, 6H). (*syn/anti*: 43/57); EI-MS (70 eV):  $m/z$  (%) = 359 [( $\text{M}^{++} + 2$ ), 6], 357 ( $\text{M}^{++}$ , 7), 260 ( $\text{M}^{++} - \text{C}_6\text{H}_9\text{O}$ , 100).

**2-((4-Chlorophenylamino)(phenyl)methyl)cyclohexanone** (Table 2, entry 5). White solid, mp 137–138 °C;<sup>56</sup> FT-IR (KBr,  $\text{cm}^{-1}$ ) 1490–1592 (C=C, aromatic), 1703 (C=O, carbonyl), 3369 (NH, second amine), 2940, 2850 (C–H, aliphatic), 3052 (C–H, aromatic); EI-MS (70 eV):  $m/z$  (%) = 315 [( $\text{M}^{++} + 2$ ), 3], 313 ( $\text{M}^{++}$ , 9), 216 ( $\text{M}^{++} - \text{C}_6\text{H}_9\text{O}$ , 85).

### 3. Results and discussion

#### Characterization of nanomaterials

The results of IR spectrum showed that all amine groups on the surface HybPOM were not linked to the  $\text{GO}-\text{Fe}_3\text{O}_4$  magnetic nanoparticle. Therefore,  $\text{H}_3\text{PW}_{12}\text{O}_{40}$  might interact with the reminded free amine groups on the surface  $\text{GO}-\text{Fe}_3\text{O}_4$  for the formation of  $\text{Go}/\text{Fe}_3\text{O}_4/\text{HybPOM}/\text{HPW}_{12}$  nanoparticles. The catalytic ability of the prepared HybPOM/HPW<sub>12</sub> and  $\text{Go}/\text{Fe}_3\text{O}_4/\text{HybPOM}/\text{HPW}_{12}$  hybrid composite was evaluated in synthesis of various  $\beta$ -amino ketones *via* Mannich reactions in aqueous media. The schematic pathway for preparation  $\text{Go}/\text{Fe}_3\text{O}_4/\text{HybPOM}/\text{HPW}_{12}$  hybrid composite is presented in Scheme 1.

IR spectra of HybPOM, HybPOM/HPW<sub>12</sub> and HPW<sub>12</sub> samples are shown in Fig. 1. The  $\text{PW}_{12}\text{O}_{40}^{3-}$  Keggin ion structure is well known and shows typical bands for absorptions at 1081 (P–O), 985 (W=O), 897 and 803 (W–O–W)  $\text{cm}^{-1}$ .<sup>41</sup> As a result, the new peaks are observed at 1079 and 962  $\text{cm}^{-1}$  in IR spectra of HybPOM/HPW<sub>12</sub> indicating that HPW<sub>12</sub> was anchored onto HybPOM successfully. IR spectra of  $\text{Go}/\text{Fe}_3\text{O}_4/\text{HybPOM}$ ,  $\text{Go}/\text{Fe}_3\text{O}_4/\text{HybPOM}/\text{HPW}_{12}$  and HPW<sub>12</sub> samples are shown in Fig. 2.

In Fig. 2, peaks at 573–630  $\text{cm}^{-1}$  in the  $\text{Go}/\text{Fe}_3\text{O}_4/\text{HybPOM}/\text{HPW}_{12}$  composite are attributed to Fe–O stretching vibration and the peak at 1080  $\text{cm}^{-1}$  is attributed to the asymmetric stretching vibration P–O.

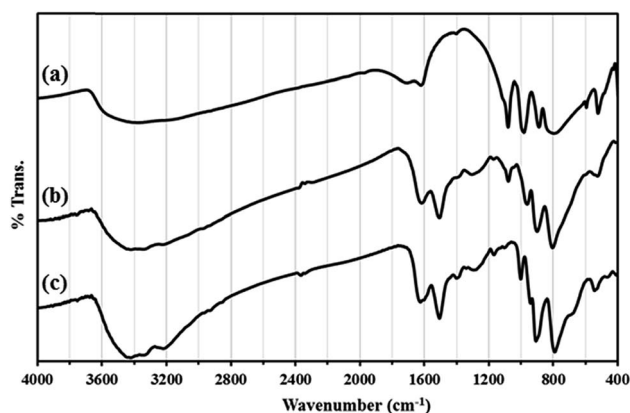


Fig. 1 IR spectra of HPW<sub>12</sub> (a), HybPOM/HPW<sub>12</sub> (b) and HybPOM (c).

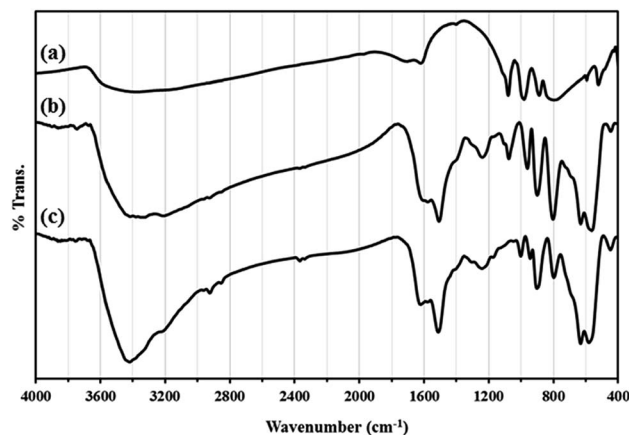


Fig. 2 IR spectra of HPW<sub>12</sub> (a)  $\text{Go}/\text{Fe}_3\text{O}_4/\text{HybPOM}/\text{HPW}_{12}$  (b) and  $\text{Go}/\text{Fe}_3\text{O}_4/\text{HybPOM}$  (c).

The XRD diffraction patterns of  $\text{Go}/\text{Fe}_3\text{O}_4/\text{HybPOM}$  (a) HybPOM/HPW<sub>12</sub> (b) and  $\text{Go}/\text{Fe}_3\text{O}_4/\text{HybPOM}/\text{HPW}_{12}$  (c) are shown in Fig. 3. X-ray diffractions pattern of HybPOM, as a typical amorphous state material is observed in the X-ray spectra of HybPOM/HPW<sub>12</sub> and  $\text{Go}/\text{Fe}_3\text{O}_4/\text{HybPOM}/\text{HPW}_{12}$ . In Fig. 3, peaks corresponding to the  $\text{Fe}_3\text{O}_4$  are observed at  $2\theta = 30.52^\circ$ ,  $35.85^\circ$ ,  $43.58^\circ$ ,  $53.96^\circ$ ,  $57.43^\circ$ ,  $63.16^\circ$  and  $74.65^\circ$  which match well with the standard  $\text{Fe}_3\text{O}_4$  sample (JCPDS file no. 19-0629).<sup>40</sup>

The peaks corresponding to HPW<sub>12</sub> at  $2\theta = 30.52^\circ$ ,  $35.85^\circ$ ,  $43.58^\circ$ ,  $53.96^\circ$ , are observed in X-ray powder diffractions of HybPOM/HPW<sub>12</sub> and  $\text{Go}/\text{Fe}_3\text{O}_4/\text{HybPOM}/\text{HPW}_{12}$  which match well with the X-ray powder diffraction pattern of  $\text{H}_3\text{PW}_{12}\text{O}_{40} \cdot 6\text{H}_2\text{O}$ .<sup>30</sup> The X-ray powder diffractions thus confirm that the Keggin structure of the HPW<sub>12</sub> compound was preserved with its immobilization on the supports.

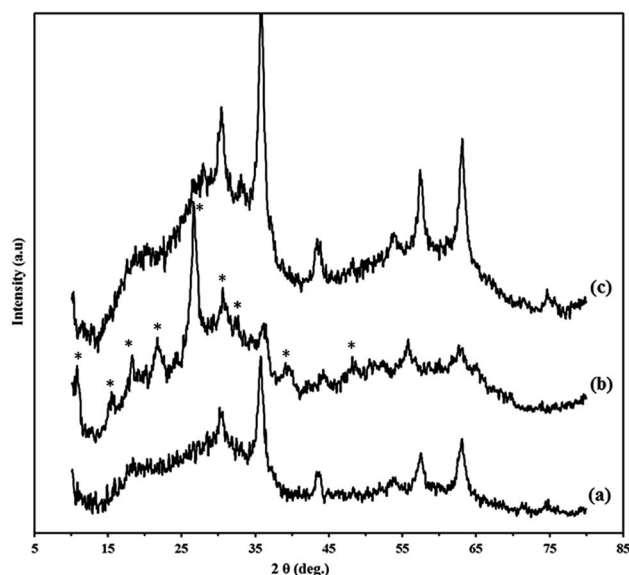


Fig. 3 The XRD diffraction patterns of  $\text{Go}/\text{Fe}_3\text{O}_4/\text{HybPOM}$  (a) HybPOM/HPW<sub>12</sub> (b) and  $\text{Go}/\text{Fe}_3\text{O}_4/\text{HybPOM}/\text{HPW}_{12}$  (c).





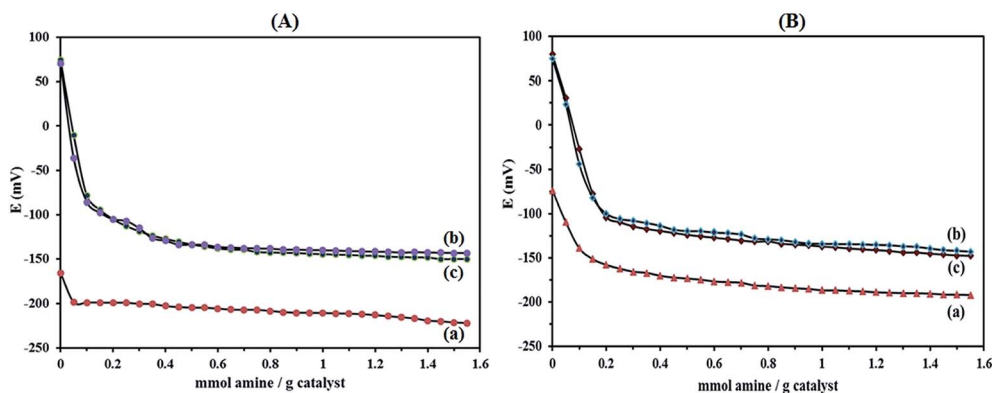


Fig. 4 The potentiometric titration with *n*-butylamine curves of (A) HybPOM (a) HybPOM/HPW<sub>12</sub> (b) HybPOM/HPW<sub>12</sub> after five consecutive runs (c); and (B) Go/Fe<sub>3</sub>O<sub>4</sub>/HybPOM (a) Go/Fe<sub>3</sub>O<sub>4</sub>/HybPOM/HPW<sub>12</sub> (b) and Go/Fe<sub>3</sub>O<sub>4</sub>/HybPOM/HPW<sub>12</sub> after five consecutive runs (c).

Numerous methods have been employed to describe the acidity of POMs in the solid state both qualitatively and quantitatively. Titration with Hammett indicators, temperature programmed desorption of adsorbed molecules such as ammonia or pyridine, adsorption microcalorimetry, NMR spectroscopy and catalytic probe reactions<sup>42</sup> are the most common methods for characterizing solid acids. The nature of the support apparently affecting the acidity of the supported HPAs by means of potentiometric titration with *n*-butylamine allows the estimation of the number of acid sites and their distribution.<sup>22</sup>

The titration curves obtained for HybPOM and HybPOM/HPW<sub>12</sub> are illustrated in Fig. 4A and those of Go/Fe<sub>3</sub>O<sub>4</sub>/HybPOM and Go/Fe<sub>3</sub>O<sub>4</sub>/HybPOM/HPW<sub>12</sub> are shown in Fig. 4B. It is believed that the initial electrode potential ( $E_i$ ) indicates the maximum strength of the acid sites and the value from which

the plateau is reached (meq. *n*-butylamine/total amount of meq. H<sup>+</sup>) indicates the total number of acid sites that are present in the titrated solid. On the other hand, the acid strength of these sites may be classified according to the following scale:  $E_i > 100$  mV (very strong sites),  $0 < E_i < 100$  mV (strong sites),  $-100 < E_i < 0$  (weak sites) and  $E_i < -100$  mV (very weak sites).<sup>43</sup> The HybPOM (Fig. 4A(a)) and Go/Fe<sub>3</sub>O<sub>4</sub>/HybPOM (Fig. 4B(a)) showed very weak and weak acid sites ( $E_i = -165.9$  and  $-73.8$  mV), respectively. Difference in the acid strength of HybPOM and Go/Fe<sub>3</sub>O<sub>4</sub>/HybPOM is attributed to the total number of free NH<sub>2</sub> groups on them. For Go/Fe<sub>3</sub>O<sub>4</sub>/HybPOM, some of the NH<sub>2</sub> groups are involved in the bonding with Go/Fe<sub>3</sub>O<sub>4</sub> nanoparticles.

As expected, the strength of the acid sites of the HPW<sub>12</sub> decreases with its addition to the HybPOM and Go/Fe<sub>3</sub>O<sub>4</sub>/

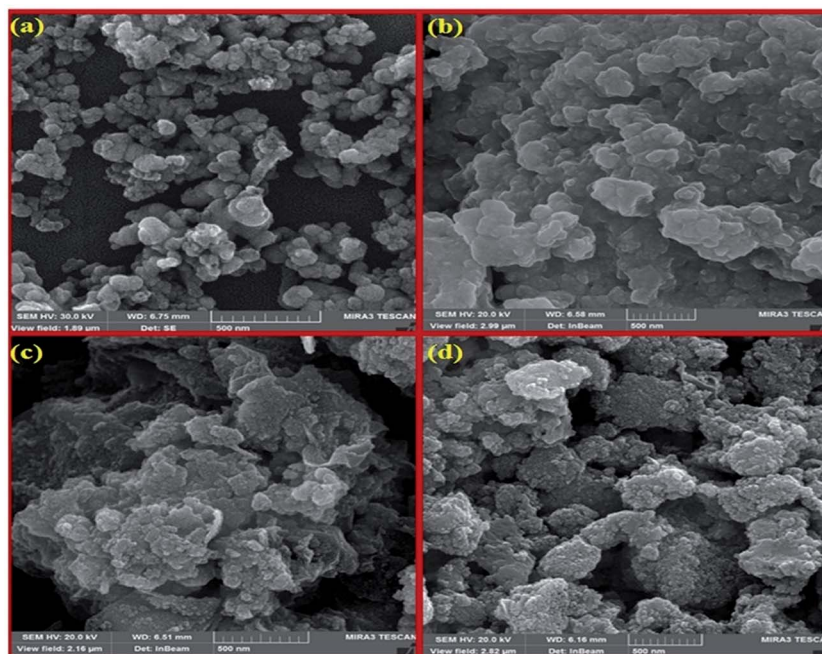


Fig. 5 The SEM images of HybPOM (a), HybPOM/HPW<sub>12</sub> (b), Go/Fe<sub>3</sub>O<sub>4</sub>/HybPOM (c) and Go/Fe<sub>3</sub>O<sub>4</sub>/HybPOM/HPW<sub>12</sub> (d).



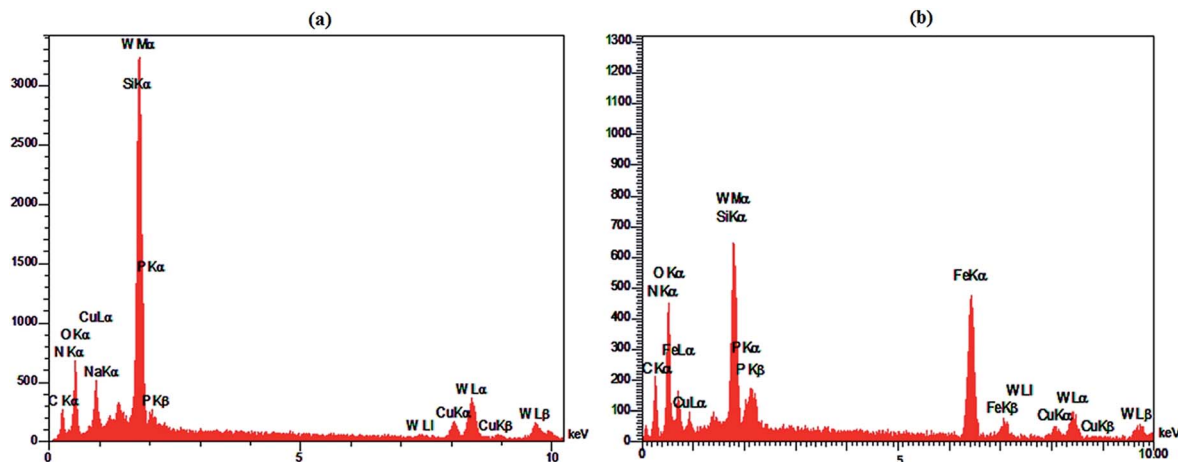


Fig. 6 EDX analysis of HybPOM/HPW<sub>12</sub> (a) and Go/Fe<sub>3</sub>O<sub>4</sub>/HybPOM/HPW<sub>12</sub> nanoparticles (b).

HybPOM surfaces. This effect depends on the extent of the interaction of HPW<sub>12</sub> with the support. According to potentiometric titration curves, HPW<sub>12</sub> presented very strong acidic sites ( $E_i = 572.2$  mV).<sup>44</sup> Potentiometric titration results of HybPOM/HPW<sub>12</sub> (Fig. 4A(b)) and Go/Fe<sub>3</sub>O<sub>4</sub>/HybPOM/HPW<sub>12</sub> (Fig. 4B(b)) samples showed the lower  $E_i$  value of 74.1 and 80 mV, respectively compared to the HPW<sub>12</sub> which might be a result of a strong interaction with the HybPOM and Go/Fe<sub>3</sub>O<sub>4</sub>/HybPOM support. Here, differences in the acid strength of HybPOM/HPW<sub>12</sub> and Go/Fe<sub>3</sub>O<sub>4</sub>/HybPOM/HPW<sub>12</sub> samples are attributed to the total number of free NH<sub>2</sub> groups on HybPOM and Go/Fe<sub>3</sub>O<sub>4</sub>/HybPOM support.

The magnetization of GO–Fe<sub>3</sub>O<sub>4</sub>, Go/Fe<sub>3</sub>O<sub>4</sub>/HybPOM and Go/Fe<sub>3</sub>O<sub>4</sub>/HybPOM/HPW<sub>12</sub> samples was measured at room temperature as shown in Fig. 5. The specific saturation magnetization of GO–Fe<sub>3</sub>O<sub>4</sub>, is 29.2 emu g<sup>−1</sup> value is smaller than the reported value of bulk Fe<sub>3</sub>O<sub>4</sub> of 92 emu g<sup>−1</sup>.<sup>45</sup> The specific saturation magnetization, of Go/Fe<sub>3</sub>O<sub>4</sub>/HybPOM and Go/Fe<sub>3</sub>O<sub>4</sub>/HybPOM/HPW<sub>12</sub> are 22.47 and 16.64 emu g<sup>−1</sup>,

respectively. A decrease in saturation magnetization observed for Go/Fe<sub>3</sub>O<sub>4</sub>/HybPOM and Go/Fe<sub>3</sub>O<sub>4</sub>/HybPOM/HPW<sub>12</sub> could be attributed to the increased mass and the loading of the HybPOM and HPW<sub>12</sub>. Even with this reduction in the saturation magnetization, complete magnetic separation of Go/Fe<sub>3</sub>O<sub>4</sub>/HybPOM and Go/Fe<sub>3</sub>O<sub>4</sub>/HybPOM/HPW<sub>12</sub> was achieved in <10 s by placing a magnet near the vessels containing the aqueous dispersion of the nanoparticles.

Fig. 6 shows the SEM images of HybPOM (a), HybPOM/HPW<sub>12</sub> (b), Go/Fe<sub>3</sub>O<sub>4</sub>/HybPOM (c) and Go/Fe<sub>3</sub>O<sub>4</sub>/HybPOM/HPW<sub>12</sub> (d). The images indicate the nano compounds after immobilization of HPW<sub>12</sub> preserved the relatively uniform spherical nanometer particles of diameter in the range 20–50 nm. EDX analysis (Fig. 7) of HybPOM/HPW<sub>12</sub> (a) and Go/Fe<sub>3</sub>O<sub>4</sub>/HybPOM/HPW<sub>12</sub> (b) nanoparticles show peaks of W, O, Si, C, N, Cu, P and C, O, Fe, W, Si, N, Cu, P respectively, the obtained element percentages of which are fairly consistent with the TGA results.

TGA was conducted in the range of 30–800 °C and the TGA plot of Go/Fe<sub>3</sub>O<sub>4</sub>/HybPOM (a) and Go/Fe<sub>3</sub>O<sub>4</sub>/HybPOM/HPW<sub>12</sub>

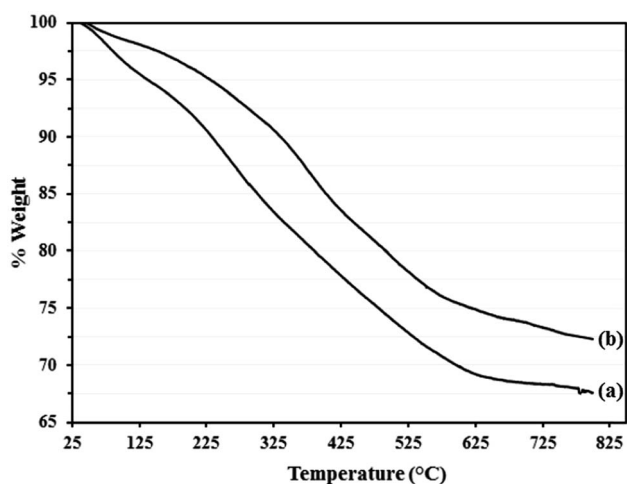


Fig. 7 TGA plot of Go/Fe<sub>3</sub>O<sub>4</sub>/HybPOM (a) and Go/Fe<sub>3</sub>O<sub>4</sub>/HybPOM/HPW<sub>12</sub> (b).

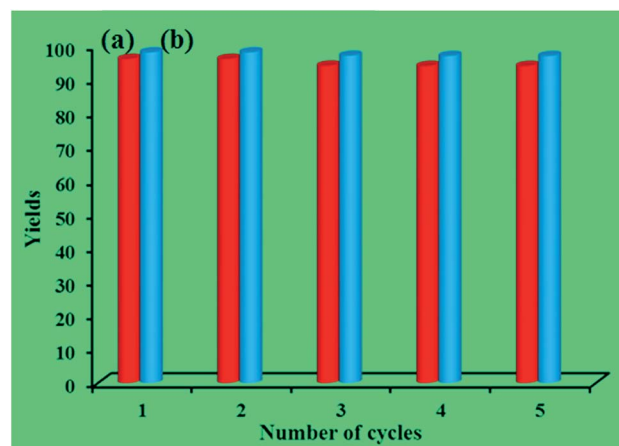


Fig. 8 The yield (%) of five consecutive cycles for the preparation of 2-(phenyl(phenylamino)methyl)cyclohexanone of HybPOM/HPW<sub>12</sub> (a) and of Go/Fe<sub>3</sub>O<sub>4</sub>/HybPOM/HPW<sub>12</sub> (b).



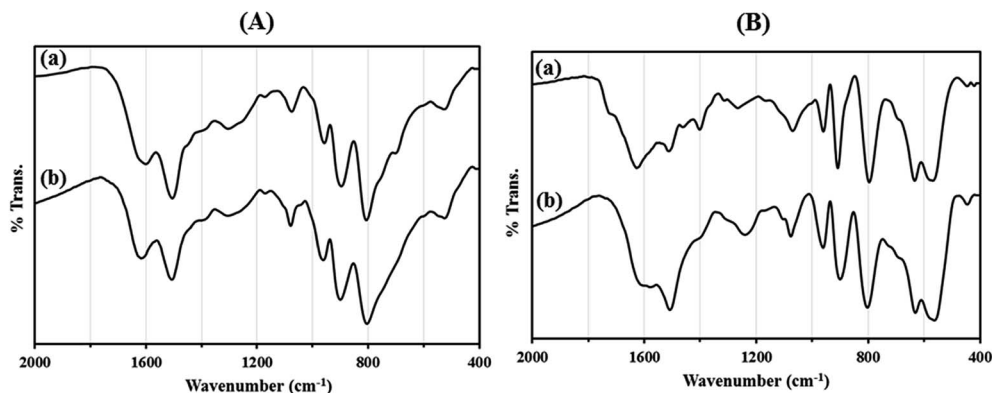


Fig. 9 The FT-IR spectra of (A) HybPOM/HPW<sub>12</sub> (a) and HybPOM/HPW<sub>12</sub> after five consecutive run (b); (B) Go/Fe<sub>3</sub>O<sub>4</sub>/HybPOM/HPW<sub>12</sub> (a) and Go/Fe<sub>3</sub>O<sub>4</sub>/HybPOM/HPW<sub>12</sub> after five consecutive run (b).

(b) are depicted in Fig. 7. Although, the TGA profile of Go/Fe<sub>3</sub>O<sub>4</sub>/HybPOM/HPW<sub>12</sub> shows continuous weight loss in the range of 30–800 °C, only three weight loss steps can be observed. The first weight loss (*ca.* 2.5%) that occurred below 150 °C is related to the loss of physisorbed water at the hybrid material surface. A main weight loss (14.00%) in the range of 150–425 °C is assigned to the decomposition of the Go/Fe<sub>3</sub>O<sub>4</sub>/HybPOM nanocomposite support.<sup>34</sup> The third weight loss (*ca.* 8.28%) in the range of 425–600 °C is due to partial decomposition of H<sub>3</sub>PW<sub>12</sub>O<sub>40</sub> (ref. 29) and residual Go/Fe<sub>3</sub>O<sub>4</sub>/HybPOM nanocomposite. The TGA analysis indicates that the prepared Go/Fe<sub>3</sub>O<sub>4</sub>/HybPOM/HPW<sub>12</sub> is thermally stable at temperatures lower than 150 °C. The total weight loss of Go/Fe<sub>3</sub>O<sub>4</sub>/HybPOM/HPW<sub>12</sub> (27.7 wt%) was less than that of Go/Fe<sub>3</sub>O<sub>4</sub>/HybPOM (32.4 wt%) because of additional residual from partial decomposition of H<sub>3</sub>PW<sub>12</sub>O<sub>40</sub>.<sup>30</sup>

Recycling experiments for catalysts were performed by the Mannich condensation of benzaldehyde, aniline and cyclohexanone in water. The model reaction was carried out by using 0.01 g of the catalysts. Fig. 8 shows the yield of five consecutive cycles for the preparation of 2-(phenyl(phenylamino)methyl)cyclohexanone in the presence of HybPOM/HPW<sub>12</sub> (a) and Go/Fe<sub>3</sub>O<sub>4</sub>/HybPOM/HPW<sub>12</sub> (b). When the reaction was completed, catalysts are separated and water was removed from the mixture to leave a residue. Then, the product was dissolved in ethyl acetate and the catalyst easily separated from the product by centrifuge or with the aid of an external magnet, followed by decantation of the product solution. The remaining catalysts were washed with ethanol and water to remove the residual product, dried under vacuum and re-used in a subsequent reaction. The catalysts have been observed to be re-usable for at least five times without

Table 1 Optimization of different parameters for the synthesis of 2-(phenyl(phenylamino)methyl)cyclohexanone catalyzed by HybPOM/HPW<sub>12</sub> (1) and Go/Fe<sub>3</sub>O<sub>4</sub>/HybPOM/HPW<sub>12</sub> (2)<sup>a</sup>

Entry	Cat. (g)	Solvent	Time (min)	Cat. 1(2)	Yield <sup>b</sup> (%) Cat. 1(2)
1	0	H <sub>2</sub> O	250(250)		Trace(trace)
2	0.003	H <sub>2</sub> O	90(110)		80(75)
3	0.005	H <sub>2</sub> O	60(90)		96(88)
4	0.007	H <sub>2</sub> O	60(55)		97(98)
5	0.007	EtOH	120(115)		89(90)
6	0.007	PEG	70(80)		70(65)
7	0.007	EtOAc	160(180)		60(88)
8	0.007	CH <sub>2</sub> Cl <sub>2</sub>	210(200)		75(85)

<sup>a</sup> Reaction conditions: aldehyde (1 mmol), amine (1 mmol), ketone (2 mmol). <sup>b</sup> Isolated yield.



**Table 2** One-pot Mannich reactions for the synthesis of  $\beta$ -amino carbonyl compounds catalyzed by HybPOM/HPW<sub>12</sub> (1) and Go/Fe<sub>3</sub>O<sub>4</sub>/HybPOM/HPW<sub>12</sub> (2)

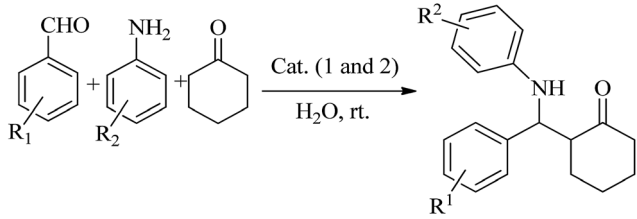
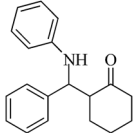
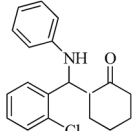
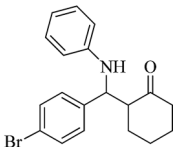
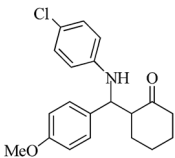
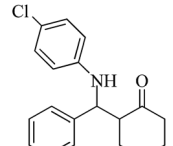
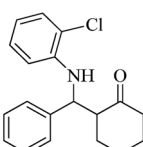
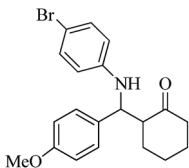
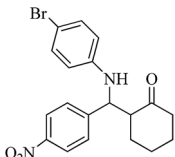
				
Entry	Product	Time (min) Cat. 1(2)	Yield <sup>a,b</sup> (%) Cat. 1(2)	Mp (°C) [ref.]
1		60(55)	96(98)	128–129 (ref. 53)
2		80(75)	92(95)	137–139 (ref. 54)
3		40(50)	90(88)	109–110 (ref. 55)
4		65(70)	94(90)	131 (ref. 56)
5		60(55)	95(96)	137 (ref. 56)
6		90(80)	92(95)	136–138 (ref. 53)
7		80(70)	90(90)	132–133 (ref. 57)
8		30(40)	97(92)	134–136 (ref. 58)





Table 2 (Contd.)

Entry	Product	Time (min) Cat. 1(2)	Yield <sup>a,b</sup> (%) Cat. 1(2)	Mp (°C) [ref.]
9		70(80)	93(95)	136–137 (ref. 57)
10		75(60)	95(98)	122 (ref. 59)
11		80(65)	90(85)	167–169 (ref. 55)
12		45(50)	93(78)	262–263 (ref. 60)
13		50(50)	95(90)	211–213 (ref. 60)

<sup>a</sup> All the products were identified and characterized by comparison of their physical and spectral data with those of authentic samples. <sup>b</sup> Isolated yield.

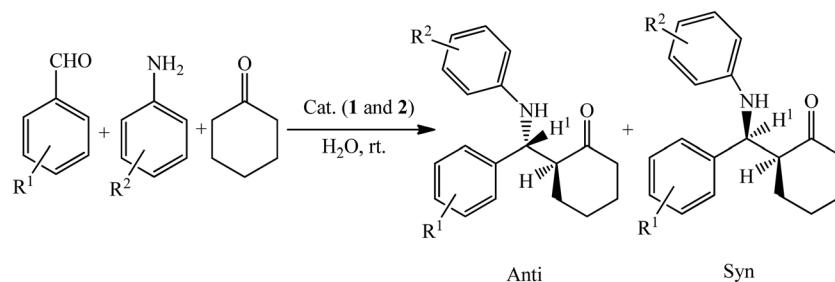
a detectable catalytic leaching or an appreciable change in activity. High catalytic activity and significantly low leaching of catalysts (during catalytic reactions) were observed by titration of acid content. The potentiometric titration curve of the re-used catalysts showed that all of their acidic sites were preserved during five cycles and HPW<sub>12</sub> leaching was negligible (Fig. 4A(c) and B(c)). The FT-IR spectra showed no significant structural changes for catalysts after five consecutive runs (Fig. 9).

### Catalytic studies

The Mannich-type reactions are very important carbon–carbon bond-forming reactions in organic synthesis and one of the

most widely utilized chemical transformations for constructing β-amino ketones and other β-amino carbonyl compounds.<sup>46,47</sup> Recently, direct Mannich reactions of aldehydes, ketones and aryl amines have been realized *via* Lewis acids, lanthanides, transition metal salt catalysis and organocatalytic approaches.<sup>47–50</sup> Most of these methods suffer from severe drawbacks including the use of a large amount of catalysts, expensive reagents or catalysts, sometimes long reaction times and low yield. The use of environmentally benign solvents in organic reactions have attracted much attention and another key research area of green chemistry, with great advances being seen in aqueous catalysis. Use of water in addition to its being



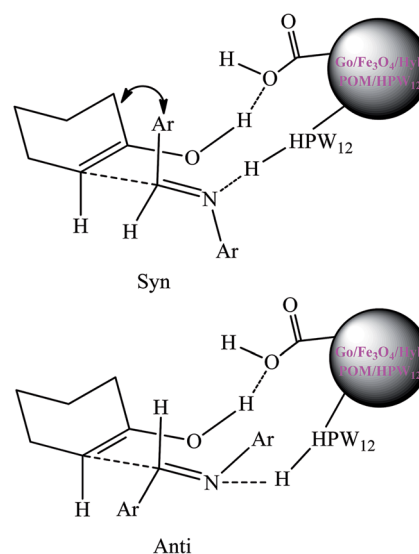


Scheme 2 Mannich reactions of aromatic aldehydes, anilines, and cyclohexanone.

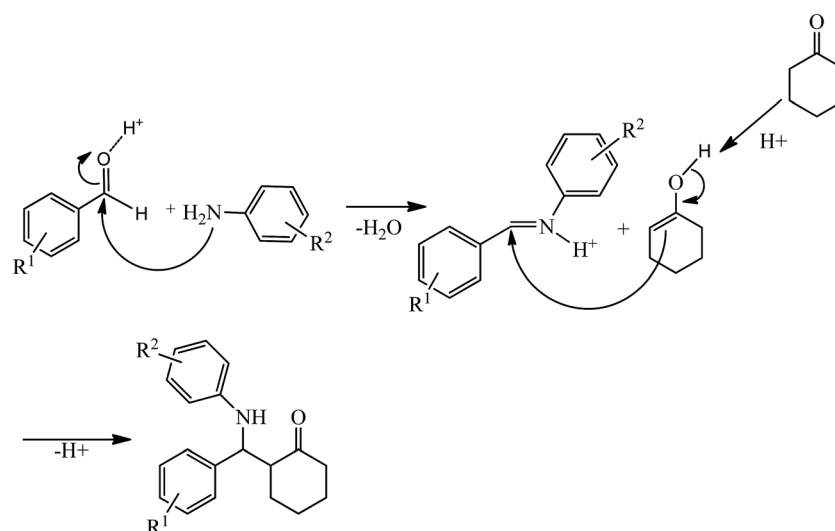
an environmentally benign solvent show unique selectivity and reactivity. In this study, the catalytic activity of HybPOM/HPW<sub>12</sub> and Go/Fe<sub>3</sub>O<sub>4</sub>/HybPOM/HPW<sub>12</sub> nanoparticles were investigated through one-pot three-component Mannich-type reactions of aldehydes, amines and cyclohexanone in water as a novel, efficient and heterogeneous catalyst under mild conditions. First, in order to optimize the Mannich-type reaction conditions, the reaction was performed with benzaldehyde, aniline and cyclohexanone as a model reaction (Table 1). As shown in Table 1, 0.005 and 0.007 g of catalysts were found to be ideal for the Mannich-type reactions and the best results were obtained using 1 mL water as solvent. The control experiments carried out using homogenous H<sub>3</sub>PW<sub>12</sub>O<sub>40</sub>·xH<sub>2</sub>O and Go/Fe<sub>3</sub>O<sub>4</sub>/HybPOM showed that the mixed Mannich product and imine were formed. When using H<sub>3</sub>PW<sub>12</sub>O<sub>40</sub>·xH<sub>2</sub>O as a homogenous catalyst, approximately 80% and 15% of the Mannich product and imine were formed, respectively. However, when Go/Fe<sub>3</sub>O<sub>4</sub>/HybPOM was used as a catalyst, approximately 65% of the Mannich product was formed. The reaction was extended to a series of aldehydes, cyclohexanone and amines to explore the generality of this catalytic system (Table 2).

The formed *anti* and *syn* isomers in the Mannich-type reactions were identified by the coupling constants (*J*) of the vicinal protons adjacent to C=O and NH in their <sup>1</sup>H NMR spectra. The

coupling constant (*J*) for the *anti*-isomer is higher than that of the *syn*. The *anti/syn* ratio was determined by <sup>1</sup>H NMR judged by the intensity of the H<sup>1</sup> (Scheme 2).<sup>51</sup>



Scheme 4 Proposed *syn*- and *anti*-intermediates for the Mannich-type reaction in the presence of Go/Fe<sub>3</sub>O<sub>4</sub>/HybPOM/HPW<sub>12</sub>.



Scheme 3 Proposed mechanism of the Mannich-type reaction in the presence of HybPOM/HPW<sub>12</sub> and Go/Fe<sub>3</sub>O<sub>4</sub>/HybPOM/HPW<sub>12</sub>.



A possible mechanism of the Mannich-type reaction in the presence of HybPOM/HPW<sub>12</sub> and Go/Fe<sub>3</sub>O<sub>4</sub>/HybPOM/HPW<sub>12</sub> as Bronsted acid catalysts is proposed (Scheme 3). The reaction proceeded typically through the imine formation of the aldehyde and amine, protonation of the imine, and the attack of the enol derived from the ketone to the protonated imine, leading to the formation of Mannich products.

As shown in Scheme 4, an intermediate are formed *via* hydrogen bonds formation among Go/Fe<sub>3</sub>O<sub>4</sub>/HybPOM/HPW<sub>12</sub>, the imine and the enol form of cyclohexanone. In the intermediate the aryl groups of aldimine and the methylene groups of cyclohexanone would be *anti* to each other and there would be less steric repulsion. Therefore, the most stable transition state would produce the *anti* isomer.<sup>52</sup>

## 4. Conclusion

The new nanoparticle catalysts were synthesized by the immobilization of H<sub>3</sub>PW<sub>12</sub>O<sub>40</sub> on the surface of H<sub>6</sub>Cu<sub>2</sub>[PPDA]<sub>6</sub>[SiW<sub>9</sub>-Cu<sub>3</sub>O<sub>37</sub>]·12H<sub>2</sub>O (HybPOM) (PPDA = *p*-phenylenediamine) organic–inorganic hybrid polyoxometalates and Go/Fe<sub>3</sub>O<sub>4</sub>/HybPOM nanocomposite. The IR spectroscopy as well as X-ray powder diffraction confirmed immobilization of H<sub>3</sub>PW<sub>12</sub>O<sub>40</sub> on the supports. Potentiometric titration results show that the new nanocatalysts possessing strong and sufficient acidic sites is responsible for excellent conversion values of products. The nanocatalysts catalyzed one-pot three-component Mannich-type reactions of aldehydes, amines and ketones in water at room temperature and the catalysts were re-used at least five times without any loss of their high catalytic activity.

## Acknowledgements

We gratefully acknowledge the Research Council of the University of Kurdistan for supporting this work.

## References

- 1 D. L. Long, E. Burkholder and L. Cronin, *Chem. Soc. Rev.*, 2007, 36.
- 2 M. T. Pope and A. Müller, *Angew. Chem., Int. Ed. Engl.*, 1991, 30, 34.
- 3 P. Kögerler and L. Cronin, *Angew. Chem., Int. Ed.*, 2005, 44, 844.
- 4 T. Yamase, *Chem. Rev.*, 1998, 98, 307.
- 5 J. T. Rhule, W. A. Neiwert, K. I. Hardcastle, B. T. Do and C. L. Hill, *J. Am. Chem. Soc.*, 2001, 123, 12101.
- 6 M. V. Vasylyev and R. Neumann, *J. Am. Chem. Soc.*, 2004, 126, 884.
- 7 N. Mizuno, K. Yamaguchi and K. Kamata, *Coord. Chem. Rev.*, 2005, 249, 1944.
- 8 N. Mizuno and M. Misono, *Chem. Rev.*, 1998, 98, 199.
- 9 M. Sadakane and E. Steckhan, *Chem. Rev.*, 1998, 98, 219.
- 10 A. Müller, P. Kögerler and A. W. M. Dress, *Coord. Chem. Rev.*, 2001, 222, 193.
- 11 T. Yamase, K. Fukaya, H. Nojiri and Y. Ohshima, *Inorg. Chem.*, 2006, 45, 7698.
- 12 J. M. Clemente-Juan and E. Coronado, *Coord. Chem. Rev.*, 1999, 193–195, 361.
- 13 D. L. Long, P. Kogerler, L. J. Farrugia and L. Cronin, *Dalton Trans.*, 2005, 1372.
- 14 D. L. Long, R. Tsunashima and L. Cronin, *Angew. Chem., Int. Ed.*, 2010, 49, 1736.
- 15 D. Volkmer, A. Du Chesne, D. G. Kurth, H. Schnablegger, P. Lehmann, M. J. Koop and A. Müller, *J. Am. Chem. Soc.*, 2000, 122, 1995.
- 16 D. W. Fan, X. F. Jia, P. Q. Tang, J. C. Hao and T. B. Liu, *Angew. Chem., Int. Ed.*, 2007, 46, 3342.
- 17 R. Neumann, *Prog. Inorg. Chem.*, 1998, 47, 317.
- 18 X. M. Yan, J. H. Lei, D. Liu, Y. C. Wu and W. Liu, *Mater. Res. Bull.*, 2007, 42, 1905.
- 19 N. Dubey, S. S. Rayalu, N. K. Labhsetwar and S. Devotta, *Int. J. Hydrogen Energy*, 2008, 33, 5958.
- 20 M. A. Alibeik, Z. Zaghaghi and I. M. Baltork, *J. Chin. Chem. Soc.*, 2008, 55, 1.
- 21 (a) T. Okuhara, N. Mizuno and M. Misono, *Appl. Catal., A*, 2001, 222, 63; (b) E. Rafiee, S. Eavani, S. Rashidzadeh and M. Joshaghani, *Inorg. Chim. Acta*, 2009, 362, 3555.
- 22 E. Rafiee, M. Joshaghani, S. Eavani and S. Rashidzadeh, *Green Chem.*, 2008, 10, 982.
- 23 *Perspectives in Catalysis*, ed. Y. Ono, J. M. Thomas and K. I. Zamaraev, Blackwell, London, 1992, p. 341.
- 24 I. V. Kozhevnikov and K. I. Matveev, *Appl. Catal.*, 1983, 5, 135.
- 25 M. Misono and N. Noriji, *Appl. Catal.*, 1990, 64, 1.
- 26 Y. Izumi, R. Hasebe and K. Urabe, *J. Catal.*, 1983, 84, 402.
- 27 H. Soeda, T. Okuhara and M. Misono, *Chem. Lett.*, 1994, 909.
- 28 M. A. Schwegler, H. van Bekkum and N. Munck, *Appl. Catal.*, 1991, 74, 191.
- 29 M. A. Wahab, I. I. Kim and C.-S. Ha, *Microporous Mesoporous Mater.*, 2004, 69, 19.
- 30 J. B. Mioc, R. Z. Dimitrijevi, M. Davidovic, Z. P. Nedic, M. M. Mitrovic and P. H. Colomban, *J. Mater. Sci.*, 1994, 29, 3705.
- 31 M. Masteri-Farahania, J. Movassagh, F. Taghavi, P. Eghbali and F. Salimi, *Chem. Eng. J.*, 2012, 184, 342.
- 32 R. Tayeb, M. M. Amini, H. Rostamian and A. Aliakbari, *Dalton Trans.*, 2014, 43, 1550.
- 33 T. A. Zillillah and Z. Li Ngu, *Green Chem.*, 2014, 16, 1202.
- 34 R. Khoshnavazi, L. Bahrami and F. Havasi, *RSC Adv.*, 2016, 6, 100962.
- 35 S. Shyles, V. Schünemann and W. R. Thiel, *Angew. Chem., Int. Ed.*, 2010, 49, 3428.
- 36 M. B. Gawande, A. K. Rath, P. S. Branco and R. S. Varma, *Appl. Sci.*, 2013, 3, 656.
- 37 A. L. Simplício, J. M. Clancy and J. F. Gilmer, *Int. J. Pharm.*, 2007, 336, 208.
- 38 I. V. Kozhevnikov, in *Catalysis for Fine Chemical Synthesis, Catalysis by Polyoxometalates 2*, ed. E. Derouane, Wiley, New York, 2002.
- 39 J. Li, S. Zhang, C. Chen, G. Zhao, X. Yang, J. Li and X. Wang, *ACS Appl. Mater. Interfaces*, 2012, 4, 4991.
- 40 B. Shen, W. Zhai, M. Tao, J. Ling and W. Zheng, *ACS Appl. Mater. Interfaces*, 2013, 5, 11383.
- 41 F. Shahbazi and K. Amani, *Catal. Commun.*, 2014, 55, 57.



- 42 W. E. Farneth and R. J. Gorte, *Chem. Rev.*, 1995, **95**, 615.
- 43 R. Cid and G. Pecci, *Appl. Catal.*, 1985, **14**, 15.
- 44 L. R. Pizzio and M. N. Blanco, *Appl. Catal.*, A, 2003, **255**, 265.
- 45 X. Yang, X. Zhang, Y. Ma, Y. Huang, Y. Wang and Y. Chen, *J. Mater. Chem.*, 2009, **19**, 2710.
- 46 G. Pandey, R. P. Singh, A. Garg and V. K. Singh, *Tetrahedron Lett.*, 2005, **46**, 2137.
- 47 L. Wang, J. Han, J. Sheng, H. Tian and Z. Fan, *Catal. Commun.*, 2005, **6**, 201.
- 48 H. Ishitani, M. Ueno and S. Kobayashi, *J. Am. Chem. Soc.*, 1997, **119**, 7153.
- 49 B. List, P. Pojarliev, W. T. Biller and H. J. Martin, *J. Am. Chem. Soc.*, 2002, **124**, 12964.
- 50 M. A. Bigdeli, M. M. Heravi, F. Nemati and G. H. Mahdavinia, *ARKIVOC*, 2008, 243–248.
- 51 (a) T. P. Loh, S. B. K. W. Liung, K. L. Tan and L. L. Wei, *Tetrahedron*, 2000, **56**, 3227; (b) C. Gennari, I. Venturini, F. Gislón and G. Schimperma, *Tetrahedron Lett.*, 1987, **28**, 227; (c) G. Guanti, E. Narisano and L. Ban, *Tetrahedron Lett.*, 1987, **28**, 4331; (d) T. Ollevier and E. J. Nadeau, *J. Org. Chem.*, 2004, **69**, 9292.
- 52 H. Wu, Y. Shen, Y. Fan, P. Zheng, C. Chen and W. Wang, *Tetrahedron*, 2007, **63**, 2404.
- 53 H. Wu, X. M. Chen, Y. Wan, L. Ye, H. Q. Xin, H. H. Xu, C. H. Yue, L. I. Pang, R. Ma and D. Shi, *Tetrahedron Lett.*, 2009, **50**, 1062.
- 54 G. Zhang, Z. Huang and J. Zou, *Chin. J. Chem.*, 2009, **27**, 1967.
- 55 M. B. Gawande, P. S. Branco, A. Velhinho, I. D. Nogueira, C. A. A. Ghumman and O. M. N. D. Teodorod, *RSC Adv.*, 2012, **2**, 6144.
- 56 E. Rafiee, S. Eavani, F. Khajooei Nejad and M. Joshaghani, *Tetrahedron*, 2010, **66**, 6858.
- 57 Y. Y. Yang, W. G. Shou and Y. G. Wang, *Tetrahedron*, 2006, **62**, 10079.
- 58 A. R. Massah, R. J. Kalbasi and N. Samah, *Bull. Korean Chem. Soc.*, 2011, **32**, 1703.
- 59 Z. Li, X. Ma, J. Liu, X. Fang, G. Tian and A. Zhu, *J. Mol. Catal. A: Chem.*, 2007, **272**, 132.
- 60 P. Vadivel, C. S. Maheswari and A. Lalitha, *Journal of Innovative Technology and Exploring Engineering*, 2013, **2**, 267.

